ELSEVIER

Contents lists available at ScienceDirect

## Computational Materials Science

journal homepage: www.elsevier.com/locate/commatsci



# Atomic column heights detection in metallic nanoparticles using deep convolutional learning



Marco Ragone, Vitaliy Yurkiv, Boao Song, Ajaykrishna Ramsubramanian, Reza Shahbazian-Yassar, Farzad Mashayek\*

Department of Mechanical and Industrial Engineering, University of Illinois at Chicago, Chicago, IL 60607, USA

ARTICLE INFO

Keywords:
Deep learning
Convolutional neural networks
Atomic column heights
Metallic nanoparticles

#### ABSTRACT

The physico-chemical and mechanical properties of metallic (e.g., Au, Pt) nanoparticle complexes highly depend on the order and the distribution of their atomic structure. While transmission electron microscopy (TEM) provides the highest spatial resolution to an image of the nanoparticle's atomic structure, it is time consuming and cumbersome to estimate the atomic column height from the two-dimensional projected TEM images. With continued progress of in-situ or operando TEM techniques in discovery of nanoscale science, it is paramount to develop artificial intelligence approaches that can be integrated with real-time TEM imaging. In this work, we present a modeling framework based upon deep learning approach (i.e., convolutional neural network - CNN) for the detection of the atomic column heights in the experimental high-resolution transmission electron microscopy (HRTEM) images of gold nanoparticles of different sizes. For this purpose, we propose a method for the generation of the training dataset based on the Wulff construction, in order to bring a physically realistic treatment to the network's learning process. Moreover, we introduce a model based on the regression scheme, as a valid alternative to a classification approach reported in the prior literature. In addition to counting atoms in verity of columns and nanoparticles, the model also provides insights concerning the experimental conditions suitable for the appropriate identification of atomic column heights by the neural network. Thus, the developed modeling approach establishes a basis for accelerated or 'on-the-fly' analysis of nanoparticles as well as a framework for extending deep learning models to broad applications in nanoscience.

#### 1. Introduction

In recent years, deep neural networks (DNN) have shown state-ofthe-art capabilities for visual recognition tasks, including the classification and the semantic segmentation of images [1]. One of the first DNN usages applied to analyze the transmission electron microscopy (TEM) for brain images segmentation is reported by Cireşan et al. [2], paving the way for further applications in the material science area. Semantic segmentation consists in the assignment of an object class label to each pixel of the image given in input to the deep learning model [3,4]. Such architectures are able to address a pixel-level fine inference and represent the natural advancement of coarse prediction networks like R-CNN, Fast R-CNN and Faster R-CNN designed for problems like bounding box object detection [5–7]. A further development in the area of semantic segmentation, is represented by fully convolutional networks (FCNs) [3]. The FCN is introduced as a reinterpretation of the state-of-the-art classification networks such as AlexNet [8], GoogleNet [9] and VGGNet [10] into fully convolutional networks for

structured prediction problems. With the aim of tackling the limitations of the state-of-the-art FCNs, Noh et al. [11] have proposed an innovative encoder-decoder architecture called Deconv-Net, where the bilinear up-sampling of FCNs has been replaced by a symmetric sequence of deconvolution and unpooling layers. Based upon the encoder-decoder principles, Ronneberger and co-workers have designed the U-Net for biomedical image segmentation [12], obtaining an outstanding performance in the 2015 ISBI competition for segmentation of neuronal structures in electron microscopy images. Badrinarayanan et al. have presented Seg-Net, an encoder-decoder network with an architecture similar to Deconv-Net and U-net, but more efficient in terms of memory requirements and computational cost [13].

In the field of materials engineering and materials chemistry, machine learning (ML) algorithms have been recently applied to predict a variety of features such as the physical properties of self-assembled materials [14], the interfacial thermal resistance between graphene and hexagonal boron nitride [15] and the on-the-fly pattern recognition of ferroelectric materials observed with an atomic force microscope [16].

E-mail address: mashayek@uic.edu (F. Mashayek).

<sup>\*</sup> Corresponding author.

Machine learning techniques have been also applied to estimate the interatomic potentials for lattice dynamics properties calculations [17], the bandgaps of different polymers with high fidelity [18,19], and the continuous cooling transformation (CCT) diagram for the heat treatment process of steel at a microstructural level [20]. Zheng et al. [21] developed a multi-channel deep convolutional network to predict the formation enthalpy of several elpasolite compounds. In particular, deep convolutional learning has become a powerful tool for the processing of experimental images of micro and nanostructures. Such images are obtained by scanning electron microscopy (SEM) [22-25], scanning transmission electron microscopy (STEM) [26] and TEM [27]. As a result, deep learning has become a promising tool for the classification of composite materials microstructures and for the extraction of local features such as defects, vacancies and chemical species. Azimi et al. [22] used a CNN model for the classification of the microstructure of low-carbon steel in SEM images. Other applications of CNN for the analysis of SEM images are reported by De Cost et al. [23], Kondo et al. [24] and Ling et al. [25], respectively for the classification of steel based on their primary microconstituents, the characterization of ceramic materials and for the featurization of SEM images of titanium, steel and synthetic powder materials. Ziatdinov et al. [26] have applied an encoder-decoder FCN on STEM images for studying the classification of defects and their structural transformation in graphene layers, characterized by the presence of vacancies and silicon (Si) dopants.

In the more recent work, Madsen et al. [27] have presented a comprehensive deep learning method for the identification of atoms in complex structures such as graphene layers with defects and metallic nanoparticles in simulated and experimental HRTEM images. Their deep learning model is developed to be stable to microscope parameters and noise, which brings segmentation-type problems to the advanced level enabling competition with the state-of-the-art experimental techniques. The algorithm is also presented as a framework with the potential of detecting the number of atoms in the individual columns of metallic nanoparticles.

While the applicability of the model for the identification of atoms has been proved in the experimental HRTEM images, the assessment of atomic column heights remains a challenge. The concern of evaluating the number of atoms in atomic columns via deep learning consists of the difficulty in estimating the actual heights in experimental images (i.e., the ground truth) for validating the predictions of the neural network. Atomic electron tomography (AET) is an efficient method to address the problem of the localization of 3D atomic coordinates in non-crystalline nano-systems. Pioneered and further developed AET based method by Miao and co-workers [28-33] enables the determination of the atomic column heights in experimental images at the sub-nanometer level. Despite the tremendous success, the AET requires a non-trivial and expensive experimental efforts to reconstruct the atomic structure observed in the TEM images. The other challenge facing experimental measurements is that nowadays, the in-situ/operando TEM imaging with ultra-fast image capturing via new directive detection cameras [34], allows to collect sequence of hundreds to thousands frames per second of the observed atomic structures, resulting in gigabytes of data per minute. However, the analysis of the resulting large dataset of images is cumbersome with the traditional techniques, such as geometric phase analysis (GPA) [35] and real phase approaches [36,37]. The main disadvantage of the conventional methods consists in the difficulty of investigating a significant amount of data in a reasonable time.

In order to tackle these challenges, in this work we propose two models based upon regression and classification methods for the detection of the atomic column heights in the experimental HRTEM images. The regression-based model is a new implementation realized in this work, whereas the classification scheme is an extension of the method presented by Madsen et al. [27]. Additionally, our current study involves a novel method for the generation of the training data set based upon the Wulff construction [38], a method for the evaluation of the equilibrium shape of a crystal in a separate phase, based on the

concept of energy minimization during cluster's formation. Finally, both the regression-based and classification models are compared to each other, providing a further boosting support to the application of deep learning for the calculation of atomic column heights in the experimental HRTEM images of nanoparticles. Thus, besides the primary objective of this work, which is the atomic column heights detection in metallic nanoparticles, a supporting objective is to improve the model fidelity and to implement it for physically realistic cases.

#### 2. Problem statement

The application of noble metal based composite in nanocatalysis and colloidal synthesis [39] has significantly increased the interest of controlling the size of metallic nanoparticles (NPs) [40,41]. The size of metal clusters is dictated by the distributions and the number of atoms in the atomic columns (atomic column heights). The most straightforward approach to predict the heights of the atomic columns is to analyze simulated and experimental STEM images, where there is a linear relationship between the intensity of the pixels and the number of atoms in the columns. Statistical methods such as statistical parameter estimation theory and other quantitative methods have been developed to determine column heights from STEM images [42-44]. On the other hand, the relationship between the pixel intensities in HRTEM images is highly non-linear and sensitive to many parameters. The state-of-the-art techniques to extract the features of the crystal structures from the experimentally acquired HRTEM images include the installment of a dedicated image corrector and the extraction of the exit wave function from a focal series. These techniques are aiming to eliminate the influence of parameters such as defocus and aberrations to fully interpret the HRTEM images. The focal series reconstruction is based on numerical methods such as the paraboloid method (PAM), the maximum likelihood (MAL) method [45,46] or the solution of the transport intensity equation (TIE) [47]. In this context, Chen et al. [36] have demonstrated that a focal series from a single projection allows to reconstruct the 3D structures of crystalline systems by counting the number of atoms in the atomic columns. However, these methods have been applied to simulated HRTEM images only. The reconstruction of a focal series in experiments requires the sample to be stable enough during the acquisition of images and uses a complex algorithm for the alignment and reconstruction of the images. Jia and co-workers [48] have implemented a scheme for the determination of the 3D shape of a nanocrystal from a single TEM image, based on the comparison between the intensities of the peaks in an experimental image of a MgO crystal and the corresponding simulated peaks. However, the framework has been applied on a well-defined layered structure, depicted from a single surface orientation [0 0 1]. The applicability of the method has not been demonstrated on more complex nanoparticles, with several crystallographic directions. Alternatively, Park et al. [49] have demonstrated that the 3D reconstruction of nanoparticles moving in a graphene liquid cell could be addressed by depicting frames of different surface orientations with TEM imaging. However, this method is not applicable to nanoparticles bounded to a solid substrate. In order to address these challenges, we have trained a deep learning model based on the CNN, to predict one of the key factors in crystal structure, the height of the atomic columns from experimentally acquired HRTEM images at a single focal level. The main advantage of data driven techniques such as neural networks, is the intrinsic independence from the physics characterizing the problem under consideration, since the learning process involves only the input data and the corresponding ground truth of the target variable. For this reason, we have assumed that a deep learning model does not require a focal series of HRTEM images as input data, whereas a single image is sufficient if the ground truth for the height of the atomic columns is available. Consequently, the learning process has been implemented on simulated images of atomic models of known ground truth, and in a successive step the model has been applied to the experimental images to predict the height of the atomic columns. In our approach, the influence of parameters such as defocus and aberrations is minimized by the implementation of a learning process based on random values of these parameters, chosen in a range which covers the experimental conditions.

Although much of the modeling approach described here could be used for broad purposes associated with TEM and SEM images processing, we focus in this paper on Au nanoparticles. Au nanoparticles perfectly suit for model development, since they possess well-defined structure and orientation for HRTEM experiments, thus can be used for further model validation and improvements. The experimentation follows the standard procedure, where a TEM grid with standard gold nanoparticle sample is mounted on a TEM holder, and 300 kV electron beam is used to perform HRTEM imaging to acquire the atomic information of gold nanoparticles. The experimental HRTEM image is then used as input to the CNN. The encoder-decoder CNN convolutes and deconvolutes the input image with the aim of finding atomic columns position and counting the number of atoms in each column.

## 3. Deep learning models

We have developed two encoder-decoder FCNs for the regression and classification tasks. Both the models in this paper build on the convolutional neural network presented by Madsen et al. [27] for the recognition of the local structure in the HRTEM images. The detailed description of the model and its architecture is given in the supplementary information and only a brief summary is provided here. The model relies on an encoder-decoder type of network, where the extraction of the features is obtained through a sequence of convolutional layers, followed by max-pooling layers [50] which reduce the size of the input image. The appropriate number and type of filters are used. The decoder (deconvolution) part aims to "restore" the image downsampled in the encoder part, using up-sampling layers and convolutional layers with the same number of filters used in the encoder part. Skipped connections between down-sampling and up-sampling layers are also used to preserve spatial information between the encoder and the decoder, as well as residual blocks to overcome the challenge of the problem of the vanishing gradient. The implemented neural network is represented in Fig. 1. While the original model [27] is built for a classification task, our implementation extends capabilities of this network by incorporating a regression-based procedure for the identification of the atomic column heights. The neural networks are built in Keras [51], an open-source library for deep learning model develop-

#### 3.1. Regression-based model

Although a standard segmentation problem is addressed with a classification framework, the specific task of the prediction of the heights of the atomic columns can be approached with a dedicated pixel-level regression model. In regression schemes, the neural network infers continuous values rather than probabilities of discrete classes. In our approach, the integer values representative of the number of atoms in the atomic columns are assigned only to the pixels located in the  $\boldsymbol{x}$ 

and y positions of the peaks, while the other pixel values decrease continuously from the center of the columns to the background. Having this in mind, our regressive neural network reconstructs the map of the column heights from the previously encoded and decoded features, using a bi-linear up-sampling convolutional layer characterized by a single 1x1 kernel [3] followed by a rectified linear activation function (ReLU) [52–54]:

$$\sigma(x) = \max(x, 0) \tag{1}$$

Eq. (1) shows the rectified linear activation function employed in the last convolutional layer of the network to compute the heights of the atomic columns in the pixel-wise regression model. The activation function takes as input the pixel values x from the last layer of the CNN and it outputs a minimum value of 0 (i.e., background), in order to avoid the problem of predicting negative column heights which do not have a physical meaning. As a result, to each pixel of the output image is assigned the value  $\sigma(x)$  of the inferred column height. Since a regression approach is used to address a semantic segmentation problem for predicting discrete values such as the atomic column heights at the peak pixels, we refer to our approach as regression-based model.

#### 3.2. Classification model

Following the state-of-the art approach, we have classified the atomic columns of the nanoparticle according to the values of their heights. Taking as input a HRTEM image of a given structure, the neural network is able to return a pre-defined number of classification maps, one of each corresponding to a column height to predict. To all the pixels belonging to a single map is attributed the probability to belong to a specific class of atomic column heights, including the background class where no atoms are present. Taking into account the dimensions and the shape of the nanoclusters observed in the experiments, we have considered that a maximum column height of 15 atoms is sufficient for our analysis. Thus, we aim to predict N = 16 output maps, where 1 map is representative of the background, while the remaining 15 correspond to different column heights in the structures we have processed. In this framework, the bi-linear up-sampling convolutional layer in the end of the neural network is characterized by 16 1x1 filters, one for each class to be inferred. In particular, the activation function implemented to compute the probabilities is the so-called softmax activation function:

$$\sigma(x_c) = \frac{e^{x_c}}{\sum\limits_{c=0}^{N} e^{x_c}}$$
(2)

The softmax activation function takes as input the pixel values  $x_c$  in the classification map c, and it outputs the probability for the portion of the map represented by  $x_c$  to belong to the class c. The scored values are normalized, so that in the final classification all the probabilities add to 1. This classification scheme follows the traditional implementation of fully convolutional networks (FCNs) for semantic segmentation tasks [3]. The classification model is presented here for the purpose of reproducing the work of Madsen et al. [27] and extending it to our problem.

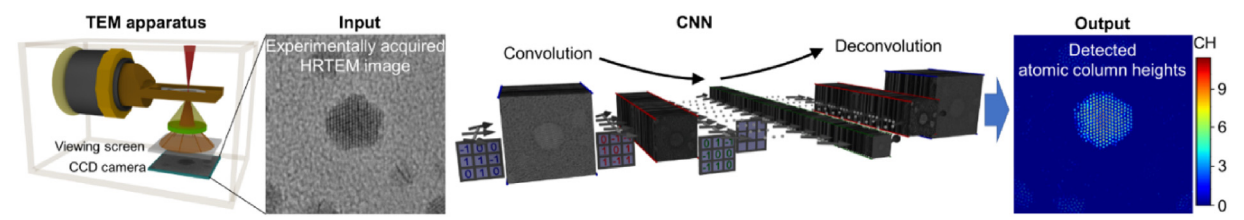


Fig. 1. Illustration of workflow followed for atomic column heights identification. The experimental HRTEM image is the input to the CNN, where convolution and deconvolution occur, and the output is the identified atomic column heights.

#### 3.3. Generation of the training and test datasets

The training and the test of the convolutional neural network has been performed on simulated TEM images of computer-generated nanoparticles, which have a high level of fidelity to the structures observed in experiments. The nanoparticles are artificially created using the Wulff construction, a method for the evaluation of the equilibrium shape of a crystal in a separate phase, based on the concept of energy minimization during particle's formation. The Atomistic Tool Kit (ATK) [55] plugin "Wulff Constructor" is used, which creates a nanoparticle with a given radius and surface energies in the main crystallographic directions. The energies of the Au surfaces are taken from Ref. [56] and are listed in Table S1 together with work function for each surface considered. Performing Wulff constructions in ATK, it is possible to create a training set of images of a particular nanoparticle varying size and shape. Since the surface energies listed in Table S1 are evaluated from the first principle DFT calculations and experimental measurements, the sizes and shapes of the resultant nanoparticles are thermodynamically consistent with the ones observed in HRTEM experiments. During the training process, the neural network learns how to evaluate the column heights of the nanoparticles generated through the physically realistic Wulff construction, resulting in a significant improvement of the reliability of the method's application to experimental images. The rotation of a particle leads to the exposure of a particular surface orientation (e.g., [1 1 0], [1 1 1] etc.), resulting in different values of column heights (Fig. 2). Depending upon the purpose, particles with different surfaces access could be mixed or used separately in the training processes. It should be noted that the Wulff construction does not take into account edge and vertex energies, which could have an influence on the shape of the nanoparticle during the HRTEM experiments. Moreover, using only one source for the generation of the training data, may lead to a bias towards a specific shape and/or orientation. For these two reasons, we have also incorporated a random insertion of atoms at the surfaces of the ideal structure generated through the Wulff construction. In this way, the training data set of simulated images contains a broad variety of nanoparticles suited for the training of the CNN. In particular, the random insertion of atoms at the surfaces allows to generate nanoparticles that are all different in size, shape, and number of atoms in each column, which is beneficial for avoiding redundancy among the samples.

The simulated structures are generated through the atomic simulation environment (ASE) [57], a python library for atomistic simulations. The corresponding simulated TEM images are created using the QSTEM code [58], through a python interface to ASE [27]. In principle, the model artificially reproduces the TEM's process to form an image of

 Table 1

 List of the microscope parameter ranges used to train the network.

Microscope Parameter	Range
Microscope Parameter  Defocus / Å  3rd-order aberration / μm  First order astigmatism magnitude /Å  First order astigmatism angle  Focal spread / Å  Electron dose / e - /Ų  c1(MTF)  c2(MTF)	Range $[-250, -150]$ $[-20, 20]$ $[0, 50]$ $[0, 2\pi]$ $[20, 40]$ $[1:10^2, 1:10^6]$ $[0, 0.01]$ $[0.5, 0.6]$ $[2.3]$
Blur Sampling, Å/pixel	[0, 2.0] [0.250, 0.265]

an observed structure, by simulating the contrast transfer function (CTF) and the modular transfer function (MTF) of the microscope. In order to take into account the variation of imaging conditions, which is always present in the experimental analysis, the microscope parameters such as defocus, spherical aberration and electron dose are randomly picked in a pre-defined range of values which are consistent with the experimental conditions. The variation of the microscope parameters allows us to take into account several effects, including the substrate and the tilt of the electron beam from a perfect zone axis. The values of the microscope parameters are listed in Table 1. The training dataset contains simulated images generated with one focal level, but the single defocus value for each image is taken randomly in a range including the experimental baseline. In addition, the generation of the images is performed on-the-fly at each step of the learning process, allowing a structure to be simulated with multiple defocus at different iterations. In this way, the model learns to predict the column heights of a given structure for a broad variation of the defocus values, providing an indirect incorporation of the focal series extraction. The neural network is invariant to the size of the input image, under the constraint that it could be divided by  $2^n$ , where n is the number of max pooling layers in the network (in our architecture n = 3). The size of the experimental images is 512x512 pixels representing an area of 132  $\pm \Delta \text{ Å}$ , where  $\Delta$ is a random number in the range between 0 and 4 Å, resulting in a resolution which lies in a range between 0.250 and 0.265 Å/pixel.

The ground truth is generated using a superposition of Gaussian distributions, centered in the positions of atoms. The choice of the values of the width of the Gaussian is particularly important since it has a significant impact on the assignment of a column to the background. Besides, in the ground truth for the regression-based model we have assigned to each pixel the value of the heights of the atomic columns.

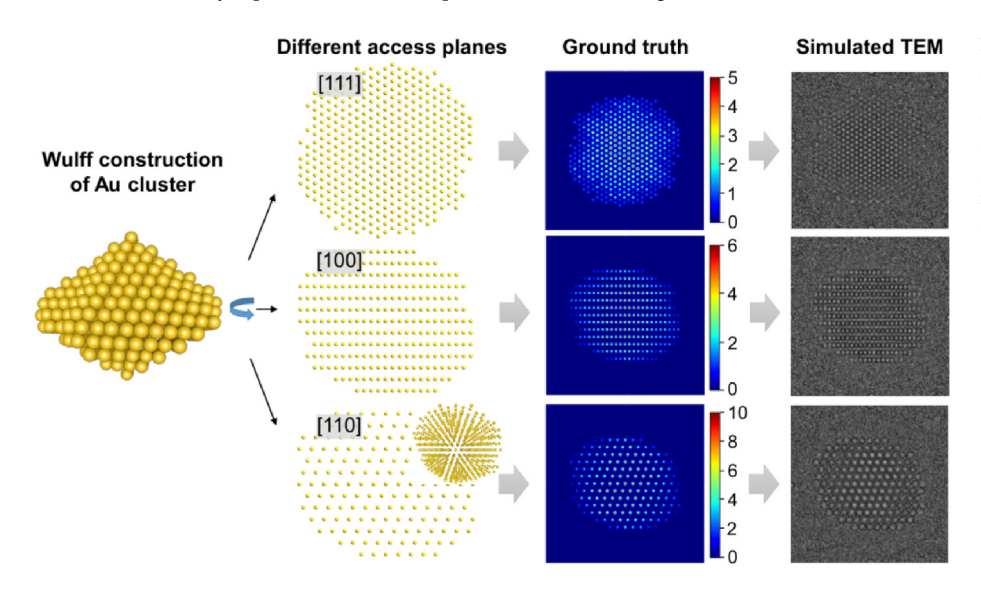


Fig. 2. Example of generation of the training data set using the Wulff construction of Au. Left – the 4 nm particle obtained during the Wulff construction using parameters from Table 1; middle panel – different access planes and the corresponding ground truth obtained by rotating the nanoparticle; right – the simulated TEM image of a particle shown on the left.

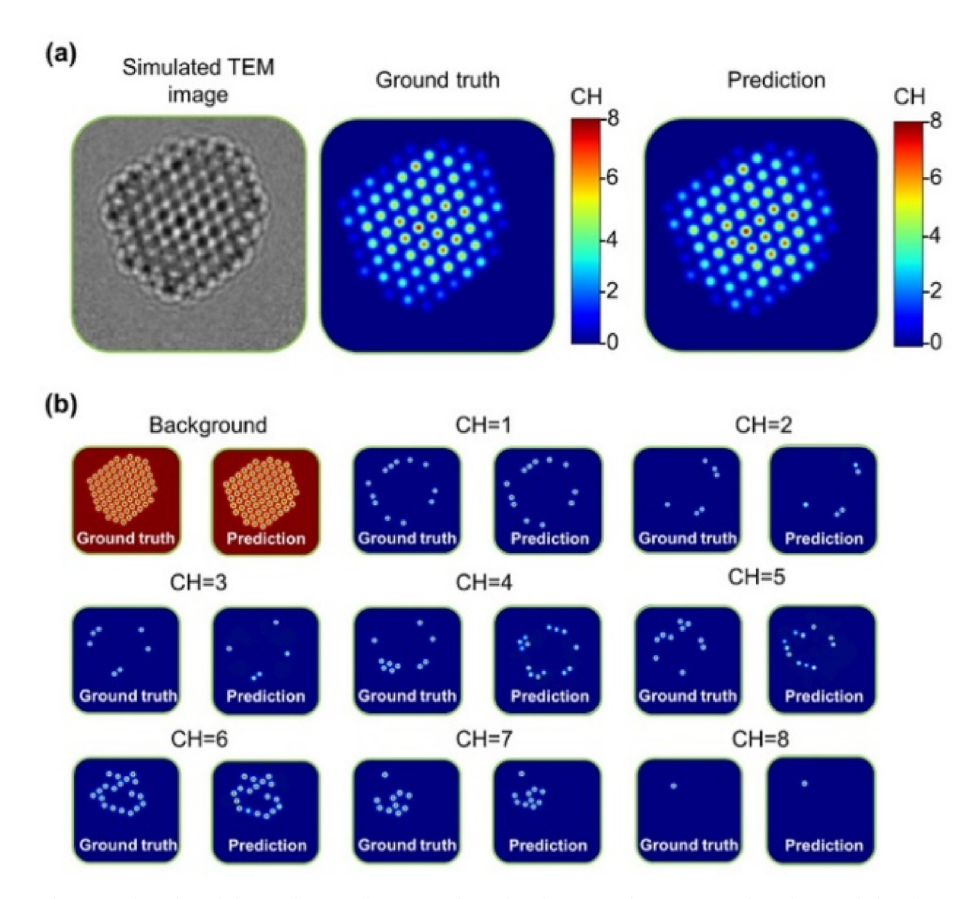


Fig. 3. Comparison between the ground truth and the prediction of atomic column heights using the regression-based (a) and classification (b) models on simulated HRTEM image. The classification model describes the probability of a column belonging to a certain class with a scale ranging from zero to one.

Since the generation of the ground truth is performed through a Gaussian distribution, the integer and discrete values representative of the number of atoms are located in the pixels corresponding to peaks (i.e., peaks of the Gaussian distribution), while the pixel values from the centers of the columns to the background decrease smoothly to zero. In this way, it is possible to create a ground truth of continuous values suitable for the application of the regression-based model. Concerning the classification model, the ground truth consists of a series of classification maps where a probability of 1 is assigned to the columns belonging to that specific height's class and 0 to the other columns and the background. Also, in this configuration, the highest value of 1 is assigned to pixels representative of the peaks, while the other pixel values exhibit a smooth decrease towards to zero at the background.

## 3.4. Models training

The models have been trained on 8000 simulated images of gold nanoparticle with the same sizes of the different structures observed in the experiments. As mentioned in the previous section, a maximum value of 15 atoms is consistent with the dimensions of the nanoparticles observed in the experimental images. In addition, the well-established technique called data augmentation has been applied to enrich the features of the training dataset. Data augmentation is a popular procedure in deep learning frameworks for image processing, which involves symmetry operations like mirroring, flipping, rotating and translating on the training images with the aim of reducing overfitting [8,9].

During each training iteration, the network learns how to estimate the column heights by the minimization of a loss function, which is different according to the model we have employed. For the purpose of regression, we have used the root mean squared error (rmse) loss function, typically implemented for regression [51] tasks. It should be noted that the root mean squared error loss function is applied at a pixel-level, and not only to the pixels corresponding to the peaks. Thereby, the proposed scheme follows a standard regression procedure at the pixel level during the learning process. On the other hand, we have applied the categorical cross-entropy [51] loss function for the classification problem. In both cases, the loss function has been regularized through the weight decay regularization [59], which is beneficial for the performance of the network since it prevents the weights to reproduce meaningful results. The model has been trained through the minibatch gradient descent (MGD) [60], using the adaptive root mean square propagation (RMSPROP) as optimizer [61]. In order to assess the correctness of the training process, the training and test learning curves are evaluated as in all deep learning frameworks. We have developed our own dedicated implementation for evaluating the accuracy of the model. For each of the 8000 structures in the training set, we have calculated the deviation of the predicted height from the value in the ground truth for each column, in order to quantify the errors in the predictions. We have evaluated the performance of the models on each image as the proportion of the number of columns predicted with the correct height. Then, we have considered the average of the results among all the generated structures, to estimate the performance on the whole training. Following this procedure, we have been able to provide a physically realistic evaluation of the reliability of the adopted framework, rather than using the standard metric provided by Keras [51] which assess a pure one-to-one comparison between the pixel values in the prediction and the ground truth. There are two reasons why for the regression-based model we have considered the proportion of the correctly predicted heights rather than the standard R<sup>2</sup> score used for regression purposes. First, the knowledge of the correctly predicted columns rather than a pure statistical

parameter like the  $R^2$  score, which lacks a physical interpretation, is more appealing for the experimentalist community. In addition, even if at a pixel level the values vary continuously as described in previous sections, the atomic column heights are integer and discrete values. Thus, the proportion of the correctly predicted peak values is a more suitable metric compared to the  $R^2$  score. The learning curve represents the trend of the accuracy of the model for each iteration of the learning process (epoch). Based on the results we have obtained, the regression-based model performs more accurately at the 18th epoch with an accuracy around 93%, while the classification network provides the highest value around 85% after 23 iterations. The results are provided in Fig. S4.

#### 4. Results and discussion

#### 4.1. Prediction on the simulated images

After training on 8000 images, we have tested the regression-based and classification neural networks using the model trained until epochs 18th and 23rd respectively, on 2000 simulated images. The procedure for the generation of the test set is identical to the one implemented for the generation of the training set. We have studied the performance of the model using the same metric adopted in the training step, based on the proportion of the correctly predicted columns in the entire nanoparticle. Fig. 3 illustrates the performance on a structure providing an accuracy which follows the results obtained in the learning curve.

Among the 75 columns of the structures shown in Fig. 3, the regression-based model correctly predicts 70 columns, leading to an accuracy of 93.3%. On the other hand, the classification model shows several errors for class 4 and 5, and one atom mismatch for class 2 and 6. Along with 65 columns predicted with the correct height, the overall accuracy is found to be 86.6%. Since we use random values of all the parameters for the generation of the training and test set, it is not straightforward to estimate a priori the best combination of parameters which could lead to a high accuracy. For this reason, we have performed a sensitivity analysis to identify the most influencing parameters. It should be noted that such a parametric study is not performed to fine-tune the model's performance towards an optimal configuration, but it is needed to estimate the performance in the application to the experimental images. The true values of the atomic column heights are not available from the experimental images, however information about the adopted microscope parameters is known from the experimentalists. Thus, evaluating the model's performance on the simulated test images varying the microscope parameters provides quantitative insights about the quality of the results obtained from the experimental images. The results are provided in supplementary information. As can be seen from Fig. S5, the defocus and the dose have the highest sensitivity, especially the lower bound of those values. Fig. 4 shows some prediction results varying the identified most sensitive parameters. Based upon this analysis, we have identified that the defocus value of around -200 Å together with the dose values higher than  $10^4 \text{ e}^-/\text{Å}^2$ provide the most accurate performing network.

Fig. 4 shows an example of HRTEM images simulated with different values of the microscope parameters and the resulting performances in the form of a deviation from the ground truth by number of atoms. In particular, Fig. 4a, b illustrate the accuracy of 60% and 76% using the highest ( $-150~\mbox{\normalfont\AA}$ ) and the lowest ( $-250~\mbox{\normalfont\AA}$ ) values of defocus, respectively. Fig. 4c, d show the comparison between different dose values while keeping the same defocus. The defocus value of  $-200~\mbox{\normalfont\AA}$  shows the best performance in the box and whiskers plot of Fig. S5, thus it is of interest to study the accuracy at this level. As can be seen, increasing the dose and keeping defocus at  $-200~\mbox{\normalfont\AA}$ , the highest accuracy of 1 is achieved.

#### 4.2. k-fold forward cross-validation

In order to further investigate the capabilities of our model, we have performed an extrapolation analysis to verify if the neural network is capable of predicting nanoparticles characterized by sizes not included in the training domain. This is an important objective towards the application to the experimental HRTEM images for which the size of the nanoparticles is not well-known. Figs. S1a-b and S2a-b in the Supplementary Information illustrate statistical distributions of the nanoparticles in the training and test based on their size. Column heights equal to 1, 4, 5, 6, 7 and 8 are the most frequent both in the training and test dataset (Fig. S1a-b) while the highest columns (11 to 15 atoms) are the least represented. This is reasonable considering the structure of the simulated nanoparticles. For example, columns with heights 4 and 5 are present in nanoparticles where the maximum height is 6, 7 or 8. In addition, nanoparticles with a maximum height between 11 and 15 include a large number of columns with height 6, 7 and 8 but also columns with height 4 and 5. Columns with height 1 are frequent because they can be found at the edges of nanoparticles of any size. The highest columns are less frequent because they represent the maximum number of atoms that can be found in the columns of the largest samples, and spherical shape nanoparticles cannot have many columns with a size equal to the maximum. However, the average column height is more or less uniform, around 150 and 40 samples per average height in the training and test datasets, respectively (Fig. S2a-b). This means that each different value of the average column height appears in more or less the same number of samples, and the only exceptions are the lowest and highest columns, which represent the tails of the distribution.

In this section, we present the application of an innovative technique which has been recently applied in materials exploration using machine learning models. Xiong et al. [19] presented a method called kfold forward cross-validation (kFCV), for which the dataset is partitioned into *k* folds of equal size containing samples with ascending/descending values of a target property. Then the cross-validation is performed in k-1 steps, where at the first step fold 1 is used for training and fold 2 for validation, at the second step folds 1 and 2 are used for training and fold 3 for validation, etc. The performance of the kFCV is evaluated using a specific metric called exploration accuracy, which is calculated as the proportion of the samples in the validation set predicted correctly in the range of the same fold. This method is promising to provide superior extrapolation capabilities to a machine learning model with respect to a traditional k-fold cross-validation for predicting materials with property values outside the training domain. We have applied a 5folds FCV to our dataset using the regression-based model, where each fold has been created by sorting the nanoparticles according to the average atomic column height, calculated as the sum of the atomic column heights in a sample divided by the number of columns in each sample and approximated to one floating point. The overall procedure is illustrated in Fig. 5.

The 5 folds are characterized by the following ranges of the average column height values: [2.2, 3.5], [3.6, 4.4], [4.5, 5.4], [5.5, 6.3] and [6.4, 8.3]. The extrapolation performance of the 5-folds FCV has been evaluated through the exploration accuracy, which is reported in the Table 2. Since at each step the model needs to be re-trained, the exploration accuracy has been evaluated at each epoch of the learning process. The learning curves for each step are shown in Fig. S3 of Supplementary Information. The learning curves show that the most accurate results are reported for the initial epochs (epoch 2 in step 1, epoch 4 in step 2, epoch 2 in step 3 and epoch 3 in step 4), with values between 75% and 81%. The values are summarized in the Table 2.

The values of the exploration accuracy tend to slightly decrease in successive steps of the 5-folds FCV, when nanoparticles with larger sizes are used for validation. However, the overall results of the exploration accuracy display that our model has satisfactory exploration capabilities and improvements towards extrapolation could further enhance the prediction of average column heights not included in the

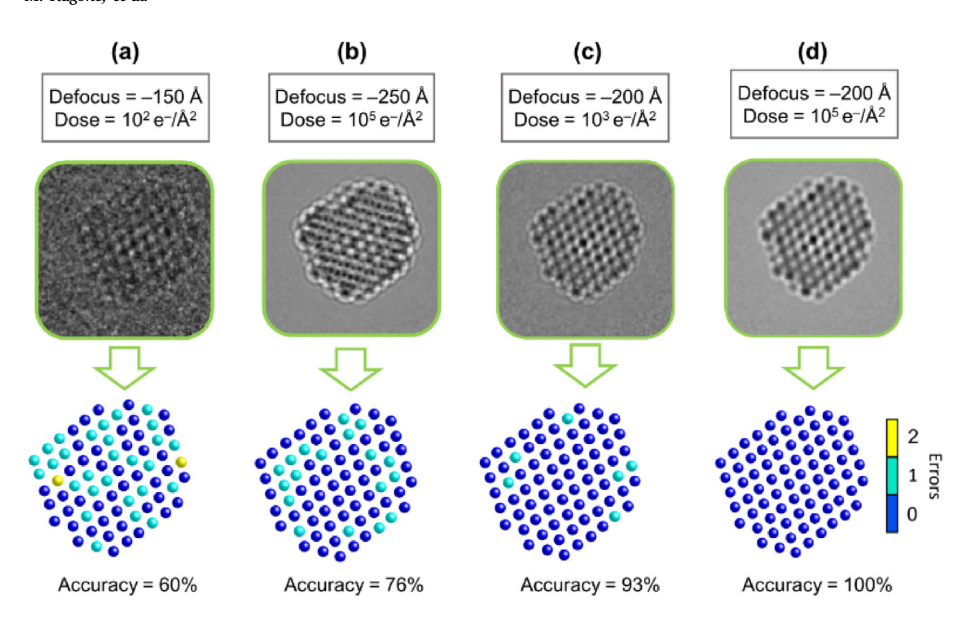


Fig. 4. Examples of model predictions on the simulated HRTEM images generated with different values of the defocus and the electron dose. (a) demonstrates the less accurate results obtained with the lowest dose. (b) illustrates how the lowest bound of the defocus range leads to a non-accurate prediction even in the case of a high dose. (c) and (d) show comparison between two dose values keeping both the defocus at  $-200 \, \text{Å}$ .

training domain.

## 4.3. Regression-based model applied to experimental HRTEM images

We first applied the regression-based CNN trained until epoch 18th to evaluate the atomic column heights in the Au nanoparticle with the relatively small size of about 2.8 nm (Fig. 6a). The experimental image together with the zoom-in is shown on the left; the middle picture depicts the model predictions, and the picture on the right illustrates plotted column heights with the contour map on the bottom plane. The model predicts atomic columns with heights from 1 to 6, where the highest columns are located in the center of (1 1 0) plane and radially decrease towards outside. This picture is used for visualization purposes only for eye guide of column heights distribution. As it is mentioned above, the quantitative evaluation of CNN predictions is not straightforward due to the lack of experimentally measured heights; however, based upon several qualitative trends we can evaluate the correctness of our predictions. In particular, considering the size of the nanoparticle (i.e., 2.8 nm) and the visible zone access (i.e., [1 1 0]), following the Wulff's construction the maximum column heights for such a nanoparticle could be 7. Our model predicts many columns with a height of

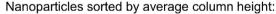
 Table 2

 Exploration accuracy at each step of the 5-fold FCV.

	step 1 FCV	step 2 FCV	step 3 FCV	step 4 FCV
Exploration Accuracy	81%	78%	76%	75%

6 in the center of the nanocluster. Taking into account the non-ideal experimental conditions and the influence of the substrate, it is reasonable to assume slightly smaller nanoparticles respect to the ideal configuration of the Wulff's construction.

We have investigated also a bigger nanoparticle with a size of 3.9 nm (Fig. 6b). Most of the columns in the center and the upper-left corner of the nanoparticle have heights equal to 10. Similar to the previous case, the column heights gradually decrease towards outside. As mentioned above, an important objective of the current study is to understand the model's limitations. A somewhat weak prediction is noticed in the upper-right corner, where a merging of two columns is present in three pairs of peaks. Since the prediction for all the other columns does not exhibit such merging, a potential source for this lack of precision could be the presence of noise in the experimental image in



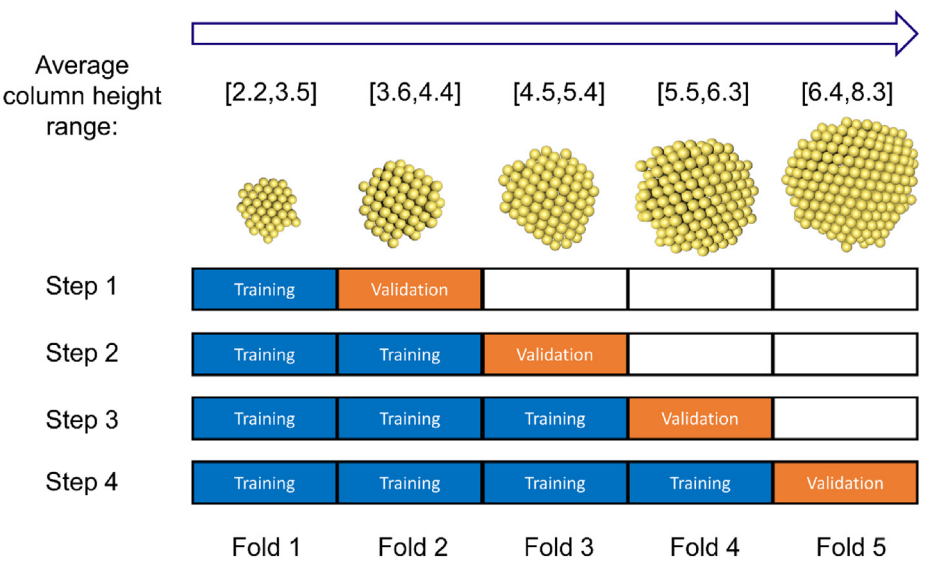


Fig. 5. 5-folds forward cross-validation for atomic column height exploration. The nanoparticles have been sorted considering the average height as the target variable and then they have been divided into 5 equally sized folds characterized by certain threshold values. The exploration ability has been tested on the validation set at each step.

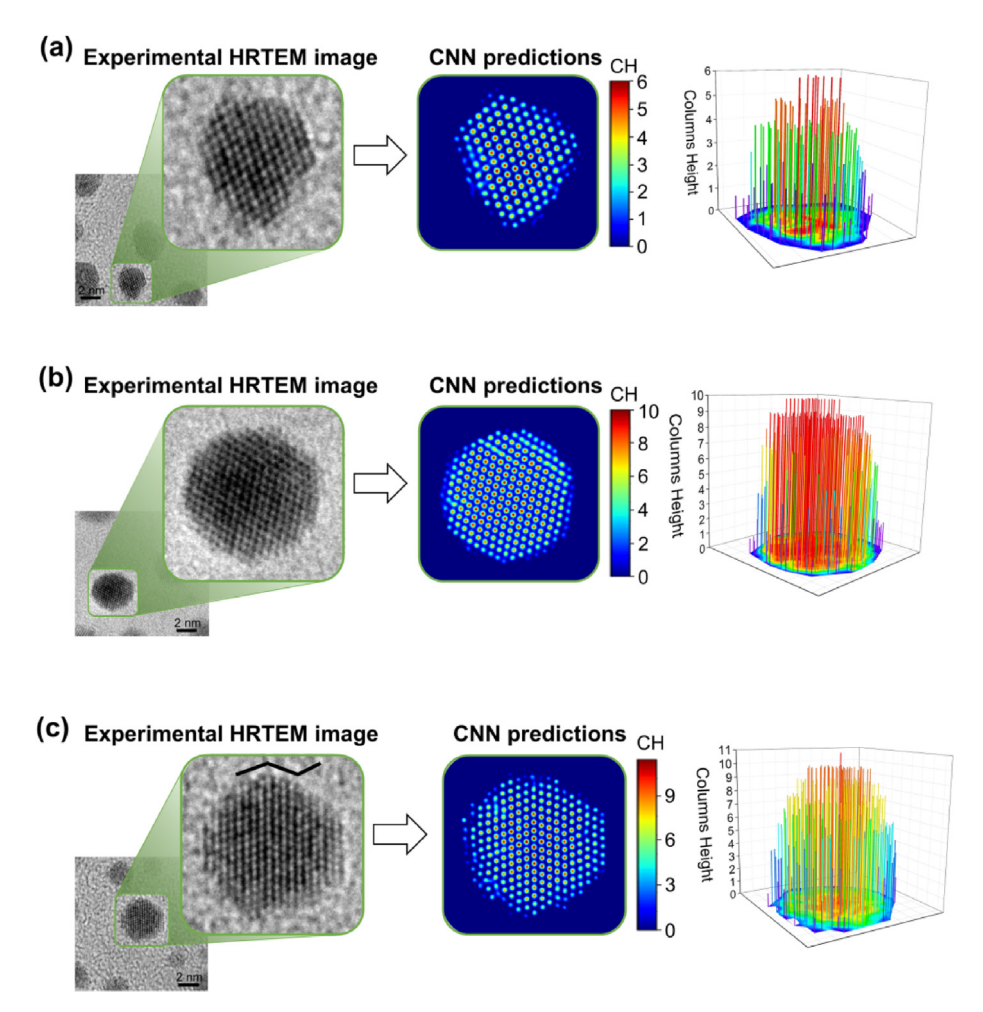


Fig. 6. CNN predictions of the atomic column heights on the HRTEM experimental image with the nanoparticle size of 2.8 nm (a), 3.9 nm (b) and 4 nm (c).

the corresponding locations of the peaks. This is a good illustration of the limitation of the model, which also provides an insight into the quality of the experimental image needed for an accurate evaluation of the CNN. It is worth mentioning that although most of the predicted columns are relatively high, our model is capable of also identifying small columns of heights 1 and 2 in the same nanoparticle.

Continuing the exploration of the model's predictive capabilities, we have applied the CNN to a relatively big nanoparticle with differently oriented surfaces (Fig. 6c). In particular, the change in orientation is shown by a black line in the enlarged picture on the left, suggesting the existence of twins. Applying the CNN, we are able to identify most of the columns and their heights revealing the maximum height of 11, as well as the twining in the particle. However, the majority of columns have heights between 8 and 10 as could be expected for this nanoparticle size.

We next present the framework for the reconstruction of a nano-particle with different surface orientations using a sequence of three consequent HRTEM images (Fig. 7). The prediction of the column height is tightly related to the intensities of the pixels in the TEM image, which depend on the orientation of the electron beam of the microscope at the moment of the acquisition. For this reason, a column depicted from a certain orientation could bias the model to an incorrect prediction of the column heights. However, considering the predictions on the HRTEM images obtained from slightly tilted angles off the zone axis, it allows to discard the heights with a non-physical meaning given their position in the nanocluster. This is particular evident in the different predictions we have obtained applying the CNN on a HRTEM image of a cluster acquired from three orientations (Fig. 7). Combining

the information of all the predictions (middle panel of Fig. 7a), it is possible to reconstruct a 3D structure of the nanoparticle (right panel of Fig. 7a). In the analyzed structure there are six sets with different number of columns, where column height 5 is the most populated.

## 4.4. Classification model applied to experimental HRTEM images

As previously discussed, in addition to a regressive network, we have also implemented a model based on the classification scheme. Although this model has been presented in prior literature [27] as a promising framework for the prediction of column heights in simulated TEM images, the applicability of this method on the experimental images is still missing. The contribution we present in this work consists of the improvement of the existing algorithm for the evaluation of the heights of the atomic columns also in the structures observed in the experiments. For the sake of comparison, we have applied the classification network trained until epoch 23rd on the HRTEM experimental image reporting the 3.9 nm cluster analyzed in the previous section. The probability scale for each predicted classification map in this image is between 0 and 1. For each column, we have assigned the heights considering the maximum probability among all the predicted classes, and then we have reconstructed the final representation of the structure (Fig. 8).

## 4.5. Comparison of the regression-based and classification networks

In the previous two sections, we have presented the evaluation of the atomic column heights in both the simulated and the experimental

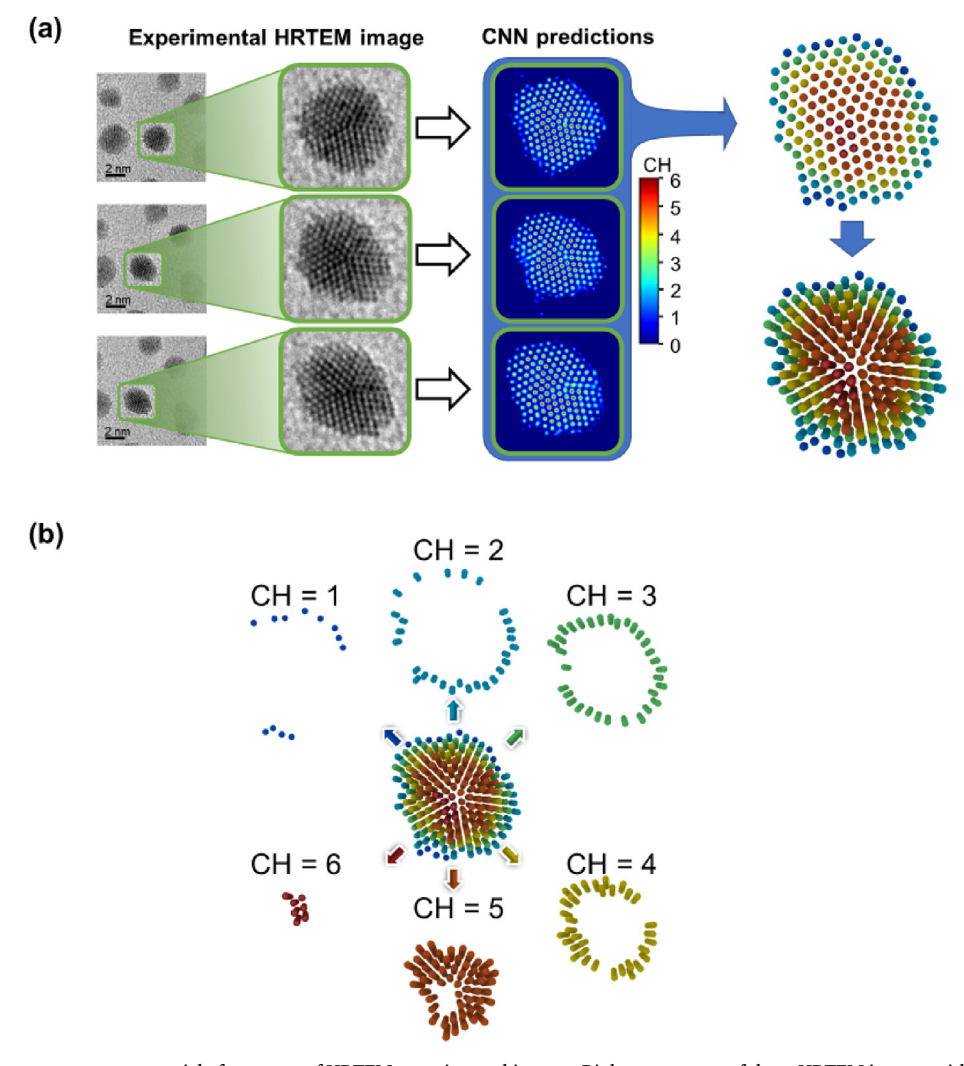


Fig. 7. A framework to reconstruct a nanoparticle from a set of HRTEM experimental images. Right – sequence of three HRTEM images with an enlargement showing a nanoparticle of interest; middle – CNN predictions of the corresponding nanoparticle; right – 3D reconstructed nanoparticle showing 2D and perspective views. The 3D structure is created from the superposition of all the predictions shown in the middle panel (a). Illustration of each separate set of column heights for the reconstructed nanoparticle (b).

HRTEM images using the regression-based and classification models. The objective is to understand the scatter between the predictions of the models on the same nanoparticle and the strategies to improve the predictions. We have first analyzed and compared the predictions on a simulated TEM, and we have found that our regressive network is more accurate than the classification network (Fig. 3). In this example we have illustrated, it is shown how the regression-based CNN fails to predict the correct height of two columns, whereas the classification CNN misclassifies a total of six columns. It would not be possible to investigate separately the results for all the samples in the training and test set; however, following the accuracy curve for training and test set

(Fig. S4) the regression-based model provides about 10% more accurate predictive capabilities than the classification model. Comparing the predictions on the experimental images (Figs. 6b and 8), we have concluded that both the models calculate values of the column heights which are physically realistic in terms of the shape and the size of the nanoparticles observed in the experiments. However, given the higher accuracy on the simulated images, we have considered that the prediction of the regression-based model is more reliable. A detailed comparison between the predictions of both models on the same experimental image shows few differences, however with an average deviation of just 1 atom. A further improvement of the present

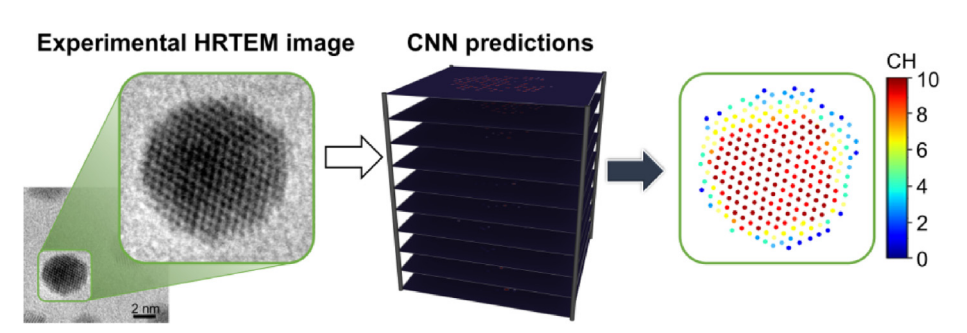


Fig. 8. CNN predictions of the atomic column heights applying classification model on the HRTEM experimental image with the nanoparticle size of 3.9 nm (left picture). All results of CNN prediction (middle picture) are shown in terms of probability of a column belonging to a certain class. The obtained atomic column heights are shown in the right picture.

framework could help in the future to eliminate the small discrepancies between the heights predicted by the two models, and to confirm how this deep learning approach is beneficial for the estimation of the atomic column heights. However, this will require detailed experimental data with known column heights (i.e., experimental ground truth).

#### 5. Conclusions

A significant progress in metallic nanoparticle research would be possible through accurate atomic column heights determination. The detection of the heights of the atomic columns is far from being achievable under realistic operating conditions. In this paper, we have presented two deep learning models to address this task in experimental HRTEM images. The first model is a regression-based convolutional neural networks, and it is presented in this work for the first time. On the other hand, the second model is based on a classification method proposed in a previous report [27] for the calculation of the heights of the atomic columns in the simulated TEM images. In order to design a deep learning framework applicable also to experimental images of gold nanoclusters, we have employed the Wulff construction of nanoparticles as an innovative method for the generation of a dataset of physically realistic structures. Different experimental HRTEM images have been used to validate the models. In particular, Au nanoparticles with varying sizes have been considered. Comparing the predictions of the regression-based and classification models, it is shown that the regression-based type algorithm performs more accurately on the simulated images. In addition, the results presented in this work provide potentially useful quantitative insights concerning the experimental requirements and operating conditions that can be valuable for the development of future deep learning algorithms. In particular, our analysis is capable to identify the range of values of the experimental parameters involved in the HRTEM experiments that allows a deep learning model to accurately predict the atomic column heights (cf., Fig. 4). Performing an extrapolation analysis using a 5-folds forward cross-validation, we have demonstrated that the regression-based model has satisfactory capabilities in exploring nanoparticles characterized by an average size not included in the training dataset. Although our models are capable of predicting column heights in different nanoparticles, the evaluation of the predictions on a particular structure requires detailed experimental information about the height of each column (i.e., ground truth). Thus, there is a great necessity to measure experimentally those structural details, which will significantly improve the predictive capabilities of the models. The atomic electron tomography (AET) method is of great promise for these purposes, however this type of analysis is beyond the primary scope of this report. Although the present work is motivated primarily by nanoparticles research, the framework is general and easily extendable to other nanoscience research related to TEM and SEM, such as catalysis, crystallography, and phase evolution analysis that would greatly facilitate the electron microscopy studies.

## 6. Data availability

The raw data required to reproduce these findings are available to download from [https://github.com/mragon2/-UIC-MIE-ESCM-ML/tree/master/ML\_ColumnHeights].

The processed data required to reproduce these findings are available to download from [https://github.com/mragon2/-UIC-MIE-ESCM-ML/tree/master/ML\_ColumnHeights].

#### Credit Authorship Contribution Statement

Marco Ragone: Methodology, Investigation, Formal analysis, Software, Validation, Visualization, Writing - original draft. Vitaliy Yurkiv: Supervision, Investigation, Validation, Visualization,

Resources, Writing - original draft. **Boao Song:** Validation, Writing - review & editing. **Ajaykrishna Ramsubramanian:** Writing - review & editing. **Reza Shahbazian-Yassar:** Resources, Writing - review & editing. **Farzad Mashayek:** Project administration, Supervision, Writing - review & editing, Resources.

#### **Declaration of Competing Interest**

The authors declare that they have no known competing financial interests or personal relationships that could have appeared to influence the work reported in this paper.

#### Acknowledgements

The authors acknowledge the financial support from the National Science Foundation award CBET-1805938. R. Shahbazian-Yassar and B. Song also acknowledge the funding from NSF-DMR-1809439. This work made use of instruments in the Electron Microscopy Service (Research Resources Center, UIC). In addition, we would like to acknowledge the NSF Extreme Science and Engineering Discovery Environment (XSEDE) award TG-DMR180055 for providing GPU resources for the results reported in this paper.

#### Appendix A. Supplementary data

Supplementary data to this article can be found online at https://doi.org/10.1016/j.commatsci.2020.109722.

#### References

- [1] Y. Lecun, Y. Bengio, G. Hinton, Nature 521 (2015) 436-444.
- [2] D. Ciresan, A. Giusti, L.M. Gambardella, J. Schmidhuber, NIPS'12 2 (2012) 2843–2851.
- [3] J. Long, E. Shelhamer, T. Darrel, IEEE Conf. Comput. Vis. Pattern Recognit. 10 (2015) (2015) 227–228.
- [4] C. Farabet, C. Couprie, L. Najman, Y. LeCun, IEEE Trans. Pattern Anal. Mach. Intell. 35 (2013) 1915–1929.
- [5] R. Girshick, J. Donahue, T. Darrell, J. Malik, CVPR'14 2 (2014) 580-587.
- [6] S. Ren, K. He, R. Girshick, J. Sun, IEEE Trans. Pattern Anal. Mach. Intell. 39 (2017) 1137–1149.
- [7] C. Szegedy, A. Toshev, D. Erhan, ICICCS-17 (2017) 1-10.
- [8] A. Krizhevsky, I. Sutskever, G.E. Hinton, Commun. ACM 60 (2017) 84–90.
- [9] C. Szegedy, W. Liu, Y. Jia, P. Sermanet, S. Reed, D. Anguelov, D. Erhan, V. Vanhoucke, A. Rabinovich, 2015 IEEE Conference on Computer Vision and Pattern Recognition (CVPR), IEEE, 2015, pp. 1–9.
- [10] K. Simonyan, A. Zisserman, 3rd IAPR ACPR (2015) 1-10.
- [11] H. Noh, S. Hong, B. Han, 2015 IEEE International Conference on Computer Vision (ICCV), IEEE, 2015, pp. 1520–1528.
- [12] O. Ronneberger, P. Fischer, T. Brox, MICCAI (2015) 234-241.
- [13] V. Badrinarayanan, A. Kendall, R. Cipolla, IEEE Trans. Pattern Anal. Mach. Intell. 39 (2017) 2481–2495.
- [14] T. Inokuchi, N. Li, K. Morohoshi, N. Arai, Nanoscale 10 (2018) 16013–16021.
- [15] H. Yang, Z. Zhang, J. Zhang, X.C. Zeng, Nanoscale 10 (2018) 19092–19099.
- [16] B. Huang, Z. Li, J. Li, Nanoscale 10 (2018) 21320–21326.
- [17] V.V. Ladygin, P.Y. Korotaev, A.V. Yanilkin, A.V. Shapeev, Comput. Mater. Sci. 172 (2020) 1093333.
- [18] A. Patra, R. Batra, A. Chandrasekaran, C. Kim, T.D. Huan, Comput. Mater. Sci. 172 (2020) 109286.
- [19] Z. Xiong, Y. Cui, Z. Liu, Y. Zhao, M. Hu, J. Hu, Comput. Mater. Sci. 171 (2020) 109203.
- [20] X. Geng, H. Wang, W. Xue, S. Xiang, H. Huang, L. Meng, G. Ma, Comput. Mater. Sci. 171 (2020) 109235.
- [21] X. Zheng, P. Zheng, L. Zheng, Y. Zhang, R. Zhang, Multi-channel convolutional neural networks for materials properties prediction, Comput. Mater. Sci. 173 (2020) 109436.
- [22] S.M. Azimi, D. Britz, M. Engstler, M. Fritz, F. Mücklich, Sci. Rep. 8 (2018) 1-14.
- [23] B.L. DeCost, E.A. Holm, Comput. Mater. Sci. 110 (2015) 126–133.
- [24] R. Kondo, S. Yamakawa, Y. Masuoka, S. Tajima, R. Asahi, Acta Mater. 141 (2017) 29–38.
- [25] J. Ling, M. Hutchinson, E. Antono, B. DeCost, E.A. Holm, B. Meredig, Mater. Discov. 10 (2017) 19–28.
- [26] M. Ziatdinov, O. Dyck, A. Maksov, X. Li, X. Sang, K. Xiao, R.R. Unocic, R. Vasudevan, S. Jesse, S.V. Kalinin, ACS Nano 11 (2017) 12742–12752
- [27] J. Madsen, P. Liu, J. Kling, J.B. Wagner, T.W. Hansen, O. Winther, J. Schiøtz, Adv. Theory Simulations (2018) 1800037.
- [28] M.C. Scott, U. Dahmen, J. Miao, R. Xu, M. Mecklenburg, B.C. Regan, C.C. Chen,

- P. Ercius, C. Zhu, Nature 483 (2012) 444-447.
- [29] C.C. Chen, B.C. Regan, M.C. Scott, L.D. Marks, Y. Huang, C.-Y. Chiu, J. Miao, C. Zhu, E.R. White, Nature 496 (2013) 74–77.
- [30] C.C. Chen, L.D. Marks, M.C. Scott, P. Ercius, Y. Yang, H. Ramezani-Dakhel, R. Xu, W. Theis, H. Heinz, M.R. Sawaya, J. Miao, C. Ophus, L. Wu, M. Bartels, Nat. Mater. 14 (2015) 1099–1103.
- [31] J. Miao, P. Ercius, S.J.L. Billinge, Science 353 (2016) 6306 aaf2157-1 aaf2157-9.
- [32] J. Zhou, Y. Yang, Y. Yang, D.S. Kim, A. Yuan, X. Tian, C. Ophus, F. Sun, A.K. Schmid, M. Nathanson, arXiv:1807.10709 (2018) 1–42.
- [33] X. Tian, D.S. Kim, S. Yang, C.J. Ciccarino, arXiv:1901.00633 (2019) 1-34.
- [34] G. McMullan, A.R. Faruqi, D. Clare, R. Henderson, Ultramicroscopy 147 (2014)
- [35] M.J. Hÿtch, E. Snoeck, R. Kilaas, Ultramicroscopy 74 (1998) 131-146.
- [36] F.R. Chen, C. Kisielowski, D. Van Dyck, Micron 68 (2015) 59-65.
- [37] P.L. Galindo, S. Kret, A.M. Sanchez, J.-Y. Laval, A. Yáñez, J. Pizarro, E. Guerrero, T. Ben, S.I. Molina, Ultramicroscopy 107 (2007) 1186–1193.
- [38] G. Wulff, Zeitschrift für Kryst. und Mineral. 34 (1901) 449.
- [39] Y. Xu, L. Chen, X. Wang, W. Yao, Q. Zhang, Nanoscale 7 (2015) 10559-10583.
- [40] B. Prasai, A.R. Wilson, B.J. Wiley, Y. Ren, V. Petkov, Nanoscale 7 (2015)
- [41] I.V. Sevonkaev, D. Herein, G. Jeske, D.V. Goia, Nanoscale 6 (2014) 9614-9617.
- [42] A.J. Den Dekker, J. Gonnissen, A. De Backer, J. Sijbers, S. Van Aert, Ultramicroscopy 134 (2013) 34–43.
- [43] S. Van Aert, A. De Backer, G.T. Martinez, B. Goris, S. Bals, G. Van Tendeloo, A. Rosenauer, Phys. Rev. B - Condens. Matter Mater. Phys. 87 (2013) 1–6.
- [44] J.M. Lebeau, S.D. Findlay, L.J. Allen, S. Stemmer, Nano Lett. 10 (2010) 4405-4408.
- [45] A. Thust, W.M.J. Coene, M. Op De Beeck, D. Van Dyck, Ultramicroscopy 64 (1996) 211–230.
- [46] W.M.J. Coene, A. Thust, M. Op De Beeck, D. Van Dyck, Ultramicroscopy 64 (1996) 109–135.

- [47] W.K. Hsieh, F.R. Chen, J.J. Kai, A.I. Kirkland, Ultramicroscopy 98 (2004) 99–114.
- [48] C.L. Jia, S.B. Mi, J. Barthel, D.W. Wang, R.E. Dunin-Borkowski, K.W. Urban, A. Thust, Nat. Mater. 13 (2014) 1044–1049.
- [49] J. Park, H. Elmlund, P. Ercius, J.M. Yuk, D.T. Limmer, Q. Chen, K. Kim, S.H. Han, D.A. Weitz, A. Zettl, A.P. Alivisatos, Science 349 (2015) 290–295.
- [50] D. Hutchison, T. Kanade, J. Kittler, J. M. Kleinberg, F. Mattern, J. C. Mitchell, M. Naor, O. Nierstrasz, C. Pandu Rangan, B. Steffen, M. Sudan, D. Terzopoulos, D. Tygar, M. Y. Vardi, G. Weikum, D. Scherer, A. Müller, S. Behnke, in: K. Diamantaras, W. Duch and L. S. Iliadis (Eds.), Artificial Neural Networks ICANN 2010, Springer Berlin Heidelberg, 6354 (2010) 92–101.
- [51] F. Chollet, 2015. https://keras.io.
- [52] K. He, X. Zhang, S. Ren, J. Sun, IEEE ICCV (2015) 1-10.
- [53] A.F. Agarap, arXiv1803.08375 cs (2018) 1-7.
- [54] B. Xu, N. Wang, T. Chen, M. Li, arXiv1505.00853 cs (2015) 1-5.
- [55] Atomistix Toolkit Version 2017.2, Synopsys QuantumWise A/S.
- [56] R. Tran, Z. Xu, B. Radhakrishnan, D. Winston, W. Sun, K. Persson, S. Ping Ong, Scientific Data 3 (160080) (2016) 1–13.
- [57] A. Hjorth Larsen, J. Jørgen Mortensen, J. Blomqvist, I.E. Castelli, R. Christensen, M. Dułak, J. Friis, M.N. Groves, B. Hammer, C. Hargus, E.D. Hermes, P.C. Jennings, P. Bjerre Jensen, J. Kermode, J.R. Kitchin, E. Leonhard Kolsbjerg, J. Kubal, K. Kaasbjerg, S. Lysgaard, J. Bergmann Maronsson, T. Maxson, T. Olsen, L. Pastewka, A. Peterson, C. Rostgaard, J. Schiøtz, O. Schütt, M. Strange, K.S. Thygesen, T. Vegge, L. Vilhelmsen, M. Walter, Z. Zeng, K.W. Jacobsen, J. Phys. Condens. Matter 29 (2017) 273002.
- [58] C. Koch, Ph.D. Thesis, Arizona State University (2002).
- [59] A. Krogh, J.A. Hertz, NIPS'91 (1991) 950-957.
- [60] M. Li, T. Zhang, Y. Chen, A.J. Smola, 20th ACM SIGKDD'14, ACM Press, 2014, pp. 661–670.
- [61] S. Ruder, arXiv1609.04747 Cs (2016) 1-10.